



Numerical investigation of starch-based granular food digestion in the duodenum: The role of duodenal posture and gastric acidity

Yifan Qin^{a,b}, Jie Xiao^{a,*}, Aibing Yu^{b,c}, Xiao Dong Chen^{a,*}

^a School of Chemical and Environmental Engineering, College of Chemistry, Chemical Engineering and Materials Science, Soochow University, Suzhou, Jiangsu Province 215123, China

^b Department of Chemical Engineering and Biological Engineering, Monash University, Clayton, Vic 3800, Australia

^c Southeast University-Monash University Joint Research Institute, Suzhou Industrial Park, Suzhou, Jiangsu Province 215123, China

ARTICLE INFO

Keywords:

Digestive reaction
Multiphase flow
Duodenum
Bioinspired reactor
Numerical simulation

ABSTRACT

Understanding digestion process in the duodenum, a complex bio-system with various unique characteristics, has been a challenge due to experimental restrictions. This work developed a comprehensive duodenal model that takes into account key features including curved geometry, pancreatic secretion and wall peristalsis. It is the first attempt to simulate dense granular flow together with pH-dependent enzymatic reactions of starch-based multicomponent particles under near-real physiological conditions. Numerical experiments enhanced our understanding of the duodenal digestive environment by analyzing the distributions of particles, enzyme and pH as well as the evolution of particle properties. The inclination of the duodenum was found to inhibit the digestive performance, even by half when completely lying down, due to a higher proportion of particles in the proximal acidic region. Additionally, a rise in gastric acidity significantly lowered the digestion rate in a lying posture, while changes in gastric acid concentration below 25 mmol/L had minimal impact in a standing case. The model developed will be valuable for optimizing food formulation, drug delivery and even the design of bio-inspired reactors.

1. Introduction

Starch-based foods, such as cereal, are major energy sources for daily activities and closely associated with human health. The digestive process in the gastrointestinal tract plays a crucial role in their bioavailability. After being ingested, starchy foods are preliminarily broken down in the mouth and stomach before entering the small intestine, where chyme is hydrolyzed thoroughly by enzymes and the final product, glucose, is absorbed through the intestinal wall. The duodenum, the first and shortest segment of the small intestine, is vital for starch digestion. α -amylase, the enzyme responsible for hydrolyzing starch into disaccharides, is primarily secreted into the digestive tract through the duodenal papilla, which is located in the descending limb of the duodenum [1]. Additionally, the duodenum serves as the pH transition section in the gastrointestinal tract. The alkaline intestinal secretions neutralize the acid chyme from the stomach, providing a favorable pH environment for α -amylase action. Furthermore, the duodenum is a complex organ with curved tubular geometry and a rich assortment of motor patterns, which also influence the digestive process.

However, our understanding of the digestion behavior in the complex duodenal system remains limited due to constraints in *in-vivo* measurements and *in-vitro* lab equipment. A complementary approach to experimental studies is the development of *in-silico* models. Compared with compartmental models [2,3], Computational Fluid Dynamics (CFD) models are capable of reproducing the details of the gastrointestinal tract as accurately as possible and providing a means to investigate transport and mixing in the gastrointestinal (GI) tract [4]. Past simulation studies have primarily focused on diverse intestinal motilities, such as peristalsis [5,6], segmentation [7,8] and pendulation [9,10]. These muscular motions have been verified to positively influence mass transfer and absorption in the intestinal tract. Reconstructing the tortuous geometry is another key modeling interest. Palmada et al., for example, generated an anatomically realistic CFD model based on CT scan slices of the duodenum [11]. Next, they validated the model against an *in-vitro* physical model with C-shaped geometry and peristaltic contractions [6].

Despite extensive modeling efforts on these physiological features, most *in-silico* experiments only ended with the analysis on mass transfer

* Corresponding authors.

E-mail addresses: jie.xiao@suda.edu.cn (J. Xiao), xdchen@mail.suda.edu.cn (X. Dong Chen).

<https://doi.org/10.1016/j.cej.2024.156965>

Received 25 August 2024; Received in revised form 4 October 2024; Accepted 20 October 2024

Available online 21 October 2024

1385-8947/© 2024 Published by Elsevier B.V.

phenomena, excluding chemical reactions. Upon entering the duodenum, partially digested food exists as a slurry of solids and liquid. Driven by intestinal motility, chyme is slowly propelled forward and mixed with digestive juice secreted from the pancreas. Pancreatic amylase permeates into porous particles and hydrolyzes the starch within. Meanwhile, alkaline secretions neutralize gastric acid, improving the pH environment for starch digestion. The digestion reaction in a region is affected by multiple factors, including substrate concentration, enzyme concentration and pH level. An independent investigation on the mixing level of a specific component, e.g., enzyme, is not sufficient to fully elucidate digestive behavior, which a common drawback of past studies.

Earlier simulation studies, such as that by Trusov et al. [12], treated each phase in the chyme as a continuum, overlooking the specific characteristics of particle behavior. In a circumstance with gravity, wet granular foods with higher density than water tend to assemble at the bottom region of a curved tubular organ and escape due to wall peristalsis. In dense particle flow, handling complex interactions between particles and the continuous phase is essential. More importantly, as porous structures composed of multiple components, starch-based particles undergo various changes during the digestive process, e.g., size, density and starch proportion [13,14]. Modelling these granular evolutions in the intestinal tract is of great significance as well.

In this study, we will develop a 3D modeling framework for the digestion of starch-based foods in the duodenum. At a first approximation, the model reproduces key duodenal details, including C-shape geometry, wall peristalsis, gastric emptying and intestinal secretion, to create a near-real physiological environment. It is important to note that nutrient absorption is not modeled since it has minimal influence on the digestion reaction and has been researched fully in the past. Beyond various environmental factors, a key contribution of this study is to characterize the complex digestive behavior of solid foods. The fluid-particle multiphase flow and the evolution of starch-based porous particles during digestion will be modelled. After model validation, it will be applied to conduct parametric studies on physiological factors, such as duodenal posture and gastric acid concentration.

2. Methods

The digestion of starch-based foods in the duodenum is a multi-physics field coupling process. Fig. 1 illustrates all the components in this model, including gastric emptying, intestinal secretion, wall peristalsis, neutralization reaction and particle hydrolysis. The foods studied are porous particles composed of starch, indigestible substrate and water. The acidic fluid mixed with particles enters the duodenum through the pylorus. Driven by wall peristalsis and gravity, the chyme moves forward and mixes with the alkaline secretion containing the enzyme. The neutralization reaction adjusts the pH that determines the enzyme activity. The starch-based particles undergo hydrolysis by the enzyme, resulting in size shrinking and porosity increase.

2.1. Geometry construction

The duodenum is approximated as a smooth C-shaped tube with a total length of L and a radius of R_0 in a relaxed state (see Fig. 2(a)). The pylorus with a radius of r_1 serves as the entrance for chyme into the duodenum. Considering the size difference between the pylorus and the duodenum, a hemispherical burst region is constructed at the front end. A secretion port with a radius of r_2 is located at the inner ring of the curved tube, at a distance L' from the pylorus. As shown in the y-z view of Fig. 2(a), the angle between the direction of gravity and the z-axis is θ , which can be adjusted to mimic different intestinal postures.

2.2. Boundary and initial conditions

The boundary and initial conditions adopted for the multiphase flow

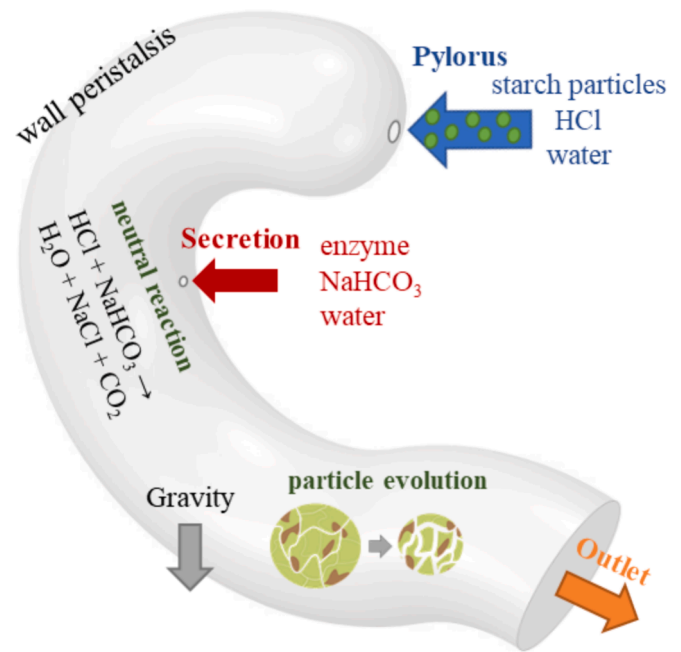


Fig. 1. A conceptual diagram of the digestion of starch-based particles in the duodenum.

simulation are illustrated in Fig. 2(b). The model features two inlets, i.e., the pylorus and the secretion port. It is assumed that the supply of chyme from the stomach remains constant. At the pylorus, the fluid with a fixed concentration of hydrochloric acid C_{HCl}^0 flows into the duodenum at a constant velocity v_p^0 . Starch-based particles, characterized by diameter d_p^0 , density ε_p^0 , indigestible ratio η_p^0 and available reaction area A_p^0 are also introduced at the pylorus with the same velocity v_p^0 and a constant mass flow rate F_p^0 . At the secretion port, a mixture of α -amylase and sodium bicarbonate with concentrations C_e^0 and $C_{NaCO_3}^0$, respectively, enters the duodenum from at a velocity v_s^0 . Although the pancreas and bile secrete a complex mix of enzymes and electrolytes, this study focuses only on the starch-digesting enzyme and the primary electrolyte. The outlet boundary condition is set to be 0 Pa gauge pressure for the fluid phase and particles are allowed to escape. The absorption of the intestinal wall is not modeled. No-slip and no-flux boundary conditions are implemented to the wall of the duodenum, and particle reflection implies no energy loss during collisions with the wall. It is assumed that the duodenal lumen is initially filled with water.

Peristalsis is the primary means of intestinal motility that propels chyme through the duodenum, causing the geometry to evolve over time (see Fig. 2(c)). In reality, it can occur throughout the small intestine and gradually diminishes after traveling a distance. In this study, peristalsis is simplified to contraction waves that initiate sequentially at the pylorus, propagate along the duodenum at a constant velocity, and eventually dissipate at the outlet. As depicted in Fig. 2(c), two or three successive contraction rings may be present in the duodenum simultaneously, followed by relaxed sections returning to their initial radius. Hence, the propulsive peristaltic wave can be represented by a piecewise function.

$$\text{if } \frac{l-ct}{\lambda} \in \left(\frac{\pi}{2} + 2N\pi, \frac{3\pi}{2} + 2N\pi \right), N \text{ is interger}$$

$$R = R_0 - A_m \cos\left(\frac{2\pi}{\lambda}(l-ct)\right)$$

else

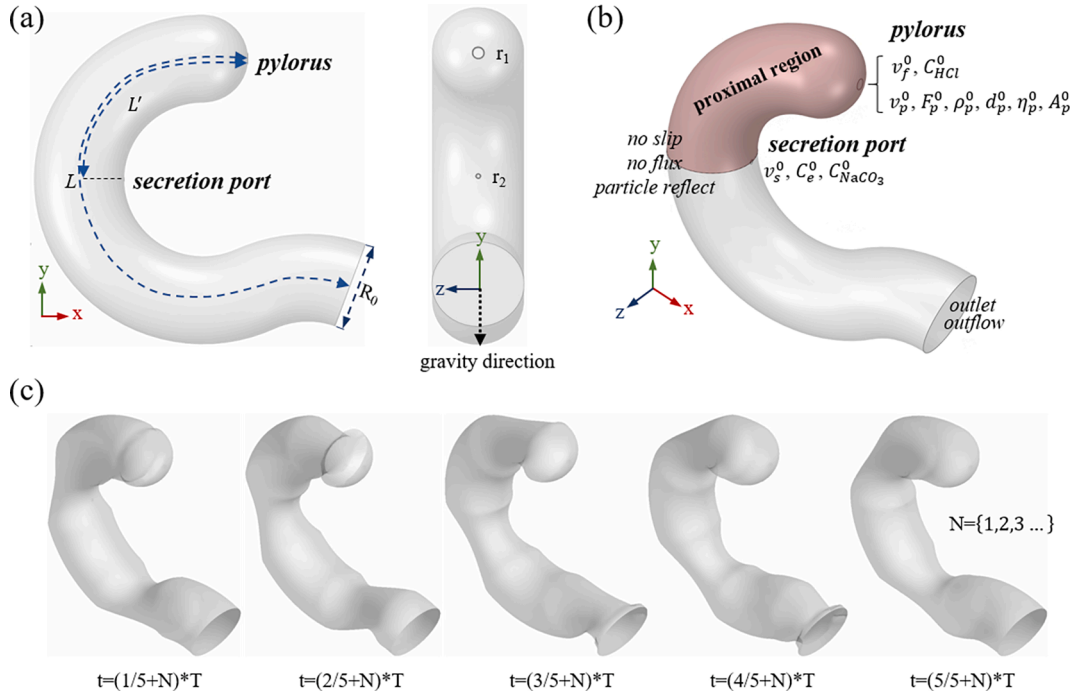


Fig. 2. Illustration of the model setting: (a) initial geometry from front and lateral views, (b) boundary conditions, (c) geometry evolution due to peristalsis.

$$R = R_0 \quad (1)$$

where R [m] is the local radial displacement of the wall from the center line. l [m], A_m [m], λ [m] and c [m/s] are respectively coordinate along the center line, amplitude of wave, wavelength and speed of wave.

2.3. Conversation equations

2.3.1. Dense discrete particle method

The dense discrete particle method (DDPM) is employed to resolve the two-phase flow of fluid and particles. This methodology is valid for dense particulate flow where the inter-particle interactions are significant. Although the overall solid volume fraction in the duodenum is not very high, particles might become extremely dense in specific regions, e. g., at the bottom. In DDPM, particles are tracked by group of parcels, each representing many particles. The inter-particle collisions are calculated indirectly using the kinetic theory of granular flow (KTGF), which is computationally less demanding. This makes DDPM a feasible approach for simulating digestive processes that occur over extended periods.

The conservation equation for the continuous phase is solved using the Eulerian multi-fluid model. In the intestine, the flow is typically considered as laminar flow. In this study, the fluid, composed of water and dissolved components, is treated as incompressible. The continuity and momentum equations are written as follows, respectively:

$$\frac{\partial}{\partial t}(\alpha_f \rho_f) + \nabla \cdot (\alpha_f \rho_f \vec{u}_f) = S_{mass} \quad (2)$$

$$\frac{\partial}{\partial t}(\alpha_f \rho_f \vec{u}_f) + \nabla \cdot (\alpha_f \rho_f \vec{u}_f \otimes \vec{u}_f) = \alpha_f \nabla p + \nabla \cdot (\bar{\tau}_f + \alpha_f \rho_f \vec{g} + K_{fp}(\vec{u}_p - \vec{u}_f) + \vec{S}_{mon}) \quad (3)$$

where α_f [-], ρ_f [kg/m³] and \vec{u}_f [m/s] denote the volume fraction, density, and velocity of the fluid phase, respectively. p [Pa] is the pressure shared by both the fluid and particle phases. $\bar{\tau}_f$ [Pa] is the fluid phase stress-strain tensor. K_{fp} represents the interphase momentum exchange coefficient. S_{mass} and \vec{S}_{mon} are the mass and momentum source

terms from the particulate phase. The particle velocity \vec{u}_p is calculated from the lagrangian approach where each particle is tracked by integrating all the forces exerted on the parcels. The governing equation of the motion for particles are written as:

$$m_p \frac{d\vec{u}_p}{dt} = m_p \frac{3\mu C_d Re (\vec{u}_f - \vec{u}_p)}{4\rho_p d_p^2} + m_p \frac{\vec{g}(\rho_p - \rho_f)}{\rho_p} + \vec{F}_{interaction} + \vec{F}_{pg} + \vec{F}_{vm} \quad (4)$$

The five terms on the right side of the equations represent the drag force, buoyancy force, interparticle interaction force, pressure gradient force and virtual mass force, respectively. For spherical particles with low particle Reynolds number, the drag coefficient C_d can be quantified by the model proposed by Gidaspow [15].

$$C_d = \frac{24}{\alpha_f Re_p} [1 + 0.15(\alpha_f Re)^{0.687}] \quad (5)$$

$$Re_p = \frac{\rho_f d_p |\vec{u}_p - \vec{u}_f|}{\mu} \quad (6)$$

The force acting on a particle resulting from interparticle interaction is computed from solid phase stress tensor given by the kinetic theory of granular flows:

$$\vec{F}_{interaction} = -m_p \frac{1}{\rho_p} \nabla \cdot \bar{\tau}_p \quad (7)$$

where $\bar{\tau}_p$ is the granular phase stress tensor. The force arises due to the pressure gradient in the fluid:

$$\vec{F}_{pg} = -m_p \frac{\rho_f}{\rho_p} \nabla \cdot \vec{u}_f \quad (8)$$

The virtual mass force, which accelerates the fluid surrounding the particle, is expressed as:

$$\vec{F}_{vm} = -C_{vm} m_p \frac{\rho_f}{\rho_p} \left(\vec{u}_p \nabla \cdot \vec{u}_f - \frac{\partial \vec{u}_p}{\partial t} \right) \quad (9)$$

where C_{vm} is the virtual mass factor. The last two forces are significant when the density of the fluid is close to that of the particles.

2.3.2. Species transport model

The mixing and transport of chemical species in the continuum phase, including the enzyme, hydrochloric acid and sodium hydrogen carbonate, are modeled by the species transport equation:

$$\frac{\partial}{\partial t}(\alpha_f \rho_f Y_i) + \nabla \cdot (\alpha_f \rho_f \vec{u}_f Y_i) = -\nabla \cdot \alpha_f \vec{J}_i + \alpha_f S_{f,i} + S_{p,i} \quad (10)$$

$$\vec{J}_i = -\rho_f D_i \nabla Y_i \quad (11)$$

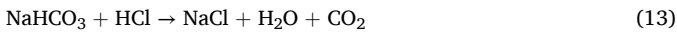
where Y_i , \vec{J}_i [kg/m²·s] and $S_{f,i}$ [kg/(m³·s)] denote the local mass fraction, diffusion flux and net production rate by chemical reaction of species i in the fluid phase, respectively. D_i [m²/s] is the diffusion coefficient for species i in the mixture. $S_{p,i}$ [kg/(m³·s)] is the net rate of heterogeneous reaction. The mixture density, which is location- and time- dependent, can be calculated based on the volume weighted mixing law:

$$\rho_f = \sum_i \rho_i y_i \quad (12)$$

where ρ_i [kg/m³] and y_i [-] are the density and volume ratio of species i , respectively.

2.4. Neutralization reaction model

The pH level in the duodenum is determined by the neutralization reaction between hydrochloric acid, a primary component of gastric acid, and sodium bicarbonate, a primary component of intestinal secretion [16]:



The mass source in the species transport equation Eq. (10) due to the homogeneous reaction in the fluid phase is proportional to the product of hydrochloric acid and sodium bicarbonate:

$$S_i = k_n C_{\text{HCl}} C_{\text{NaCO}_3} \quad (14)$$

where k_n is the rate constant of the neutralization reaction [L/(mol·s)]. S_i is negative for the reagents and positive for the reaction product. Molar concentration of the i -th component C_i [mol/L] is obtained by the following equation:

$$C_i = \frac{Y_i \rho_f}{M_{w,i}} \quad (15)$$

where $M_{w,i}$ [g/mol] is the molar mass of the i -th component.

The local pH level is calculated by a piecewise formula based on the concentration of the excess component, either hydrochloric acid or sodium bicarbonate [17].

$$\text{pH} = \begin{cases} -\lg \frac{C_{\text{HCl}} + \sqrt{C_{\text{HCl}}^2 + 4K_w}}{2} & C_{\text{HCl}} > C_{\text{NaCO}_3} \\ -\lg \sqrt{\frac{K_{pH,1}(K_{pH,2} C_{\text{NaCO}_3} + K_w)}{K_{pH,1} + C_{\text{NaCO}_3}}} & C_{\text{HCl}} < C_{\text{NaCO}_3} \end{cases} \quad (16)$$

where $K_{pH,1}$ [mol/L] and $K_{pH,2}$ [mol/L] are the first and second dissociation constants of carbonic acid, respectively. K_w [mol²/L²] is the ion product of water. The enzyme α -amylase, which acts on starch, is very sensitive to pH level. The pH-dependent activity of α -amylase can be calculated by the following empirical function [18]:

$$\alpha = \frac{1}{1 + \frac{10^{-\text{pH}}}{K_{a1}} + \frac{K_{a2}}{10^{-\text{pH}}}} \quad (17)$$

Here $K_{a1} = 10^{-5.878}$ and $K_{a2} = 10^{-8.873}$, which were obtained by fitting the above equation against the experimental data from literature [19]. The fitting result is given in [Supplementary Material, Fig. S1](#).

2.4.1. Particle hydrolysis model

The mass source from the enzymatic reaction of starch-based particles is described by a modified form of an established particle hydrolysis model [20]. It accounts for both diffusion and hydrolysis occurring on the surface and within the interior of porous particles, leading to reductions in particle size and starch proportion. However, solving the diffusion equation for a large number of particles over a transient process is highly complex and demands excessive computing resources. Our recent work has demonstrated that diffusion resistance within a particle is negligible for the intestinal digestion of cooked rice particles when the initial size is less than 0.5 μm [21]. Consequently, the diffusion of solutes, i.e., enzyme and maltose, within a particle can be neglected, provided the initial particle size is sufficiently small (e.g., 0.1 μm).

The rate of starch hydrolysis in a particle Q_p [kg/s] can be expressed as the sum of the surface reaction rate Q_{sur} [kg/s] and the internal reaction rate Q_{int} [kg/s]

$$Q_p = Q_{sur} + Q_{int} \quad (18)$$

$$Q_{sur} = \frac{V_{max} A_p (1 - \eta_p) (1 - \varepsilon_p) C_e \alpha}{K_m + C_e} \quad (19)$$

$$Q_{int} = \frac{V_{max} A_i V_p (1 - \eta_p) C_e \alpha}{K_m + C_e} \quad (20)$$

where V_{max} [kg/(m²·s)], K_m [mol/L], A_p [m²], A_i [m⁻¹] and V_p [m³] are the maximum rate of product formation per unit area, equilibrium constant, external surface area, internal surface area per unit particle volume and particle volume. η_p [-] represents the ratio of indigestible components and can be calculated using the following equation based on the initial ratio.

$$\eta_p = \eta_p^0 \frac{1 - \varepsilon_p^0}{1 - \varepsilon_p} \quad (21)$$

Here ε_p [-] is the porosity of a particle where pores are filled with water. ε_p^0 and η_p^0 are their initial values.

$$\varepsilon_p = \frac{\rho_s - \rho_p}{\rho_s - \rho_f} \quad (22)$$

where ρ_s [kg/m³] and ρ_f [kg/m³] denote the densities of the solid and liquid phases, respectively. ρ_p [kg/m³] is the granular density, which decreases due to the internal reaction.

$$\frac{\partial \rho_p}{\partial t} = - \left(1 - \frac{\rho_f}{\rho_s} \right) \frac{Q_{int}}{V_p} \quad (23)$$

It implies that the space occupied by the solid component will be progressively replaced by liquid during the digestive process. The change in the mass of a particle results from both surface and internal reactions.

$$\frac{\partial m_p}{\partial t} = -Q_{sur} - \left(1 - \frac{\rho_f}{\rho_s} \right) Q_{int} \quad (24)$$

Then the diameter and volume of a particle can be computed by

$$d_p = \sqrt[3]{6V_p/\pi} = \sqrt[3]{6m_p/(\rho_p\pi)} \quad (25)$$

The mass transfer rate of maltose from the discrete phase to the continuous phase is computed by summing the mass sources from all particles in a cell zone:

$$S_{p,m} = \sum_{j=1}^{N_p} \kappa_{sm} Q_p \quad (26)$$

where κ_{sm} denotes the mass increase ratio when converting starch to maltose (162:171). Likewise, the mass source term in the continuity equation Eq (1) is the sum of granular mass changes in a cell zone:

$$S_{mass} = - \sum_{j=1}^{N_p} \frac{\partial m_p}{\partial t} \quad (27)$$

2.5. Quantitative analysis

Given the variability in the mass of reactive substrates, i.e., starch, in the duodenum due to continuous injection and discharge of particles, evaluating the digestive environment based solely on the hydrolysis rate is inadequate. Therefore, a digestion rate coefficient $k_{dig}[s^{-1}]$, representing the digestion rate per unit mass of starch, is introduced to provide a more rigorous assessment.

$$k_{dig} = \frac{Q_{p,sum}}{M_{s,sum}} \quad (28)$$

The total digestion rate $Q_{p,sum}$ [kg/s] in the duodenum is given by adding up the starch hydrolysis rates in all particles:

$$Q_{p,sum} = \sum_{j=1}^N Q_{p,j} \quad (29)$$

The total starch mass $M_{s,sum}$ [kg] in the duodenum is calculated based on the mass and properties of each particle.

$$M_{s,sum} = \sum_{j=1}^N M_{p,j} \left(\frac{(\rho_{p,j} - \rho_w) \rho_s}{(\rho_p^0 - \rho_w) \rho_{p,j}} \left(1 - \frac{\eta_p^0 (\rho_p^0 - \rho_w)}{\rho_{p,j} - \rho_w} \right) \right) \quad (30)$$

where $M_{p,j}$ [kg] and $\rho_{p,j}$ [kg/m³] are the mass and density of the j -th particle. ρ_w [kg/m³] and ρ_s [kg/m³] are density of water and starch, respectively. η_p [-] is the ratio of indigestible component in a particle. The superscript “0” denotes the initial state of a particle.

The distribution of particles is a crucial factor for elucidating the digestive environment throughout the duodenum. To quantitatively compare particle distributions in different cases, the proportion of particles in the proximal duodenum at time t , denoted as P_t , is counted. The proximal duodenum is defined as the segment prior to the secretion port, as marked in red in Fig. 2(b).

Data collection at the outlet of the computational domain allows us to examine how the duodenal passage influences particle evolution. The residence time of a particle, t_{res} , is determined by its entry and exit times. The hydrolysis ratio of a particle upon exiting the outlet is computed based on its initial and final properties.

$$H_{p,out} = 1 - \left(1 - \frac{\rho_p^0 - \rho_p}{(1 - \eta_p^0)(\rho_p^0 - \rho_w)} \right) \left(\frac{d_p}{d_p^0} \right)^3 \quad (31)$$

2.6. System specifications

The parameters for the duodenum geometry, peristalsis movement and inlet conditions at the pylorus and secretion port are based on the average physiological data. The specific values used in the base case simulation are listed in Table 1. Given the variability in gastric emptying rates for different meals [22], the rate of cooked rice particles injected at the pylorus is set to 1×10^{-5} kg/s, equivalent to 36 g emptied per hour. Materials properties at body temperature (37 °C) are provided in Table 2. The initial size of particles upon injection into the duodenum was 0.1 mm, which is sufficiently small to neglect solvent diffusion

Table 1

Values of physiological parameters used in the simulation.

	Parameter	Value	References
Geometry	Length L	25 cm	[25]
	Radius R_0	2 cm	[25]
Pylorus	Radius r_1	2.5 mm	[26]
	Flow velocity v_f^0	0.007 m/s	[27]
	Concentration of HCl C_{HCl}^0	10 mmol/L	[24,28]
	Particles injection rate F_p^0	1×10^{-5} kg/s	–
Secretion	Distance from pylorus L'	9.6 cm	[29]
	Radius r_2	1 mm	[30]
	Flow velocity v_s^0	0.01 m/s	[31]
	Concentration of NaHCO ₃ $C_{NaCO_3}^0$	100 mmol/L	[31]
	Concentration of enzyme C_e^0	26.5 mmol/L	[32]
Peristalsis	Amplitude of wave A_m	6.65 mm	[33]
	Wavelength λ	10 cm	[33]
	Speed of wave c	2 cm/s	[16]

resistance around the particle. The diffusivity of α -amylase is computed by the Einstein-Stokes equation, with the diameter of 7 nm [23].

Beyond the base case, 29 additional cases were designed for an orthorhombic parametric study, varying the leaning angle and the acid concentration from the stomach. Specifically, the leaning angle (θ) investigated were 0°, 22.5°, 45°, 67.5° and 90°, which alter the direction of the gravitational force as described in Table 3. The acidity of the gastric solution varies significantly with dietary factors and meal timing, with pH levels in the distal gastric compartment typically ranging from 1.5 to 3 [24]. Six concentrations of hydrochloric acid C_{HCl}^0 , 5, 10, 15, 20, 25 and 30 mmol/L were therefore chosen for further study.

2.7. Numerical implement

The meshing and simulation were carried out using ANSYS Fluent software. For the transient simulation, the phase coupled SIMPLE scheme was employed for pressure-velocity coupling and the least squares cell-based method was used for spatial discretization to ensure efficient convergence. The convergence criterion requires the residuals of all equations to be below 1×10^{-3} . Automatic local cell remeshing was enabled to maintain stable dynamic mesh calculations. The mesh was reconstructed at every time step when cells marked for remeshing were detected. The time step was set to 0.002 s. Mesh independence analysis was conducted by testing five different meshing schemes (see Supplementary Material, Fig. S2). A scheme with 73,811 mesh elements was adopted. The computational time for an 800 s simulation is approximately six days.

3. Results and discussion

3.1. Base case analysis

Fig. 3 illustrates in detail the evolutions of starch-based particle digestion and the digestive environment in the duodenum. The simulation was conducted for 800 s to allow the system to reach a steady state. Fig. 3(a, b & c) plot the total starch mass, total starch digestion rate and average digestion rate coefficient in the duodenum calculated using Equations (28), (29) & (30). Fig. 3(d, e & f) display the distributions of pH, enzyme concentration and particle density at four representative sampling times. The colormap for enzyme concentration is presented on a logarithmic scale, while the colormaps for pH and particle density are






Table 2

Values of physicochemical properties in the simulation.

	Parameter	Value	References
Cooked rice particles injected at the pylorus	Diameter d_p^0	0.1 mm	—
	Porosity ϵ_p^0	0.5	[20]
	Indigestible ratio η_p^0	0.2	
	Available internal area A_p^0	1.39×10^5 m ² /m ³	
	Maximum reaction rate V_{max}	1.3×10^{-5} kg/(m ² s)	
	Michaelis constant K_m	1×10^{-4} mol/L	
α -amylase	Molecular Weight	226.2 g/mol	Estimated by Einstein-Stokes equation
	Diffusivity	1.75×10^{-11} m/s ²	
maltose	Molecular Weight	342.3 g/mol	[34]
	Diffusivity	4.5×10^{-10} m/s ²	
hydrochloric acid	Molecular Weight	36.5 g/mol	[35]
	Diffusivity	7×10^{-9} m/s ²	
sodium bicarbonate	Molecular Weight	84 g/mol	[35]
	Diffusivity	1.75×10^{-9} m/s ²	
sodium chloride	Molecular Weight	58.4 g/mol	[36]
	Diffusivity	1.5×10^{-9} m/s ²	
carbon dioxide	Molecular Weight	44 g/mol	[37]
	Diffusivity	2.2×10^{-9} m/s ²	
Values used in Eq. (14)–(17)	Neutralization kinetic constant k_n	2.56×10^7 M ⁻¹ ·s ⁻¹	[35]
	First constant of carbonic acid dissociation $K_{pH,1}$	4.9×10^{-7} mol/L	[17]
	Second constant of carbonic acid dissociation $K_{pH,2}$	5.62×10^{-11} L/mol	[17]
	pH-dependent parameter of enzyme activity K_{a1}	$10^{-5.878}$	[19]
	pH-dependent parameter of enzyme activity K_{a2}	$10^{-8.873}$	[19]

Table 3

Different duodenal postures implemented by altering the direction of the gravity.

Leaning angles	0°	22.5°	45°	67.5°	90°
Gravity direction (x, y, z)	(0, -1, 0)	(0, -0.92, -0.38)	(0, -0.71, -0.71)	(0, -0.38, -0.92)	(0, 0, -1)
Illustration of posture					

on a linear scale.

At the early feeding stage (from 0 s to 60 s) in Fig. 3(a), the mass of starch in all injected particles is directly proportional to the simulation time due to the constant injection rate. However, as shown in Fig. 3(b), the hydrolysis rate is initially limited. This phenomenon can be explained by the visual distribution maps (see Fig. 3(f)). At 10 s, most particles are located in the proximal segment, where the enzyme concentration is extremely dilute and the enzyme activity is inhibited by the acidic environment. As time progresses, the hydrolysis rate throughout the duodenum climbs significantly, which is driven by triple factors. The major mechanism is an increasing number of particles in the bottom

region where both the pH and enzyme concentration are favorable for the hydrolysis reaction (see Fig. 3(d, e & f)). Secondly, the excessive secretion of sodium bicarbonate neutralizes hydrochloric acid from the stomach, expanding the areas with high enzyme activity (see Fig. 3(d)). Besides, the enzyme secreted from the midpoint of the duodenum gradually spreads throughout the entire domain (see Fig. 3(e)). The average digestion rate coefficient in Fig. 3(c) represents the average digestive environment surrounding the particles. Its rapid rise in the initial stage indicates an increasingly higher proportion of starch being hydrolyzed in regions with more favorable enzyme activity and concentration.

After 60 s, the increase in the rate coefficient slows down. It suggests that, although the number of particles in the duodenum continues to rise, the digestive environment (specifically enzyme concentration and pH level) remains basically stable in the bottom region where most particles reside. In other areas, the distributions of these factors keep evolving. Particularly in the proximal duodenum, the intestinal secretion containing the enzyme and alkaline electrolytes are transported along the outer ring of the C-shaped tube. Around 400 s, the curves of starch mass and digestion rate in Fig. 3(a & b) begin to plateau, signing the homeostasis of the duodenal system.

Fig. 4 displays the residence time and starch hydrolysis ratio of particles exiting the duodenum between 600 and 800 s. The information collected in this steady period can be extrapolated to represent the whole digestion process, which lasts several hours. A total of 33,049 particles were captured. Regression analysis shows a positive linear relationship between the hydrolysis proportion and the residence time in the duodenum. The average residence time was found to be 211 s. For comparison, the transit time of non-disintegrating capsules in the human duodenum, tracked using magnetic markers, ranged from 7 to 245 s [38]. Worsøe et al. also applied a similar noninvasive tool, which could display the position and orientation of a magnetic pill in the body, to assess the small intestinal transit time [39]. Based on their data, Nagar et al. calculated the transit velocity along the intestine, finding the magnitude in the duodenum to be around 1.5×10^{-3} m/s, comparable to the average value from this simulation case (1.1×10^{-3} m/s) [40]. Additionally, Wright et al. estimated that the front of a testing solution (methylene blue) took about 122 s to pass through an *in-vitro* duodenum model [41]. The higher average value obtained in this simulation is attributed to the nature of particle flow. The escape of wet porous particles, which are denser than water, from the bottom region of a curved tube require overcoming gravity, thereby increasing transit time.

The average digestion rate coefficient during the steady stage (600 ~ 800 s) is 1.88×10^{-3} s⁻¹. The average starch hydrolysis ratio in particles exiting the duodenal is 28 %. Due to the operational challenges and ethical restrictions of human experiments, direct evidence from previous publications to validate the simulation data is lacking. However, these results could be indirectly proven through animal experiments or *in-vitro* gastrointestinal simulators. For instance, Martens et al. examined *in-vivo* starch digestion kinetics in four small-intestinal segments of growing pigs, finding hydrolysis ratios of 28 % for ground barley and 19 % for ground maize in the first segment (i.e., duodenum and proximal jejunum) [14]. The digestion kinetics constant obtained from an *in-vitro* simulated gastrointestinal study using chewed, cooked rice grains was approximately 1.6×10^{-3} s⁻¹ [42], which is very close to the simulated value. Gonzalez et al. investigated the digestion of starch dispersions in an *in-vitro* intestinal model using a dialysis membrane, estimating a digestion rate coefficient for potato starch at 6.17×10^{-4} s⁻¹ [43]. The higher digestion rates observed in this simulation may result from the fact that the computational case used cooked rice, which is more sensitive to enzymatic action and has more pores for hydrolysis compared to the uncooked starches used in the referenced experiments.

3.2. Effect of duodenal posture

The posture of the duodenum varies with human body posture and

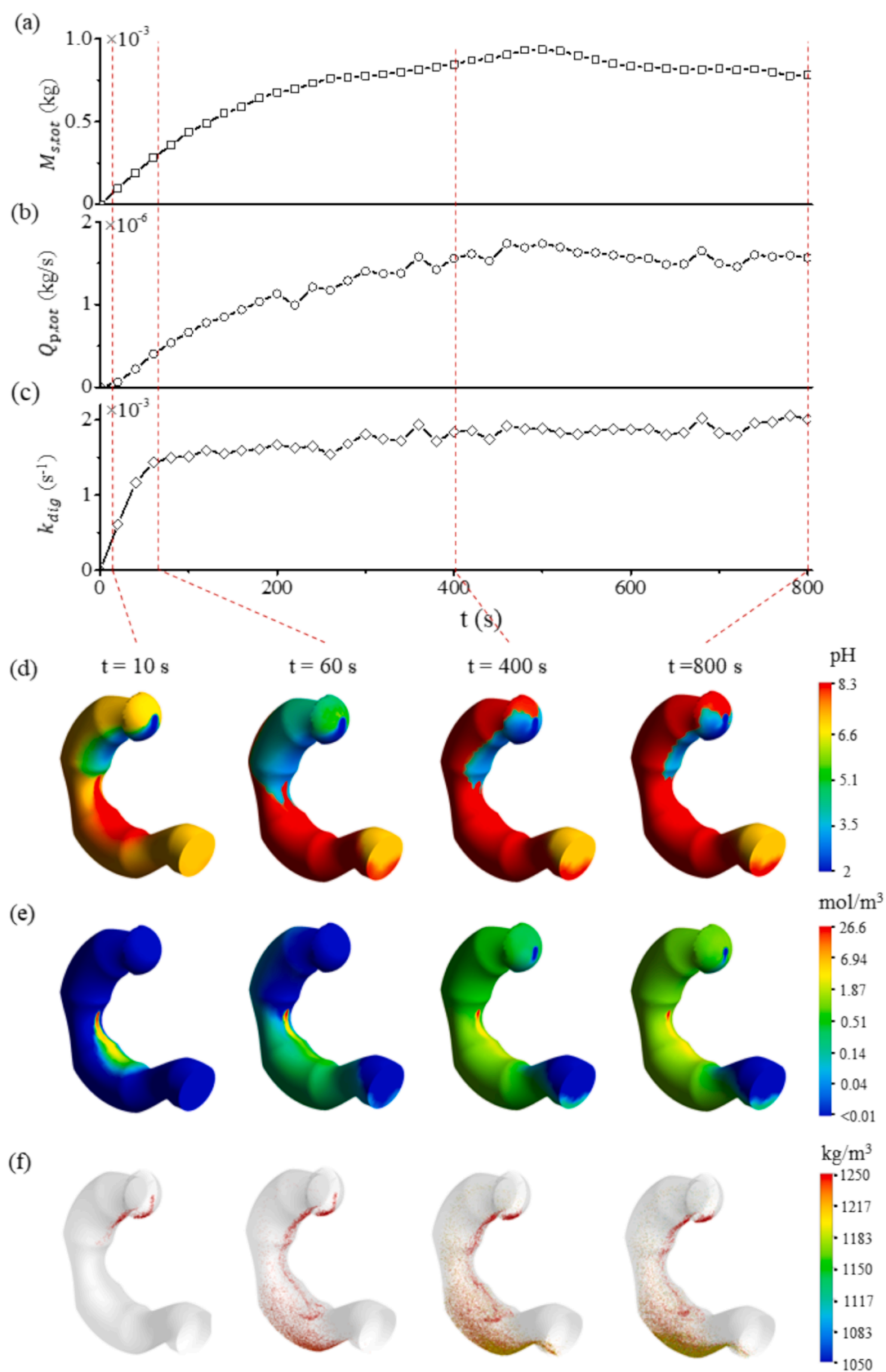


Fig. 3. Simulation results of base case. (a) total starch mass, (b) total starch digestion rate, (c) digestion rate coefficient, (d) pH distribution, (e) enzyme distribution, and (f) particle distribution.

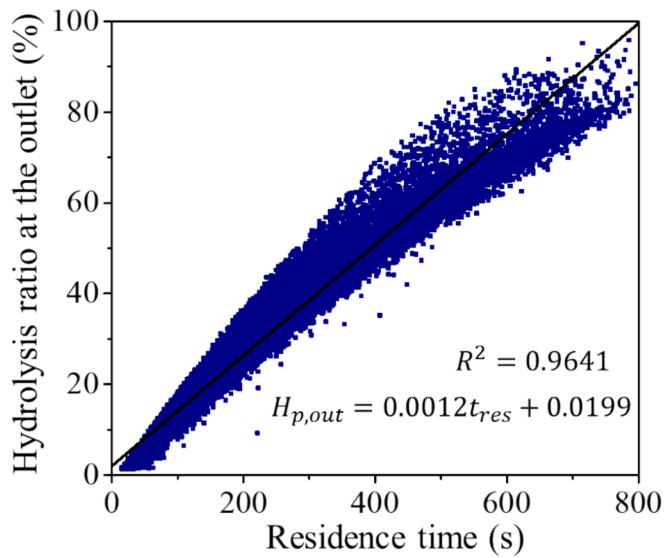


Fig. 4. Relationship between particle residence time and starch hydrolysis ratio at the duodenal outlet.

individual anatomical differences. To investigate the impact of posture on digestion, simulations were conducted by changing the leaning angle as specified in Table 3 while keeping all other parameters consistent with the base case. Fig. 5 presents the simulation results for different postures. As detailed in the previous section, the evolution of the digestion rate coefficient over time is plotted in Fig. 5(a). The results indicate that lying down leads to an extremely low digestion rate in the early stage because the inclination delays the contact between starch

particles and the secreted juice. After a period of rapid growth, the system with a completely lying posture (i.e., 90°) stabilizes, whereas the other cases (i.e., 0°, 22.5°, 45°, 67.5°) enter a phase of gradual increase in the digestion rate coefficient. From 600 s to 800 s, all five groups fluctuate around a fixed level, which declines as the leaning angle goes up.

The average coefficient \bar{k}_{dig} over this period for each posture is calculated and shown in Fig. 5(b). It clearly demonstrates a negative linear relationship with the leaning angle. The completely lying posture restrains the average coefficient by nearly half compared to the standing posture. Fig. 5(c) depicts the spatial distributions of pH and particles in the duodenum at 800 s, shedding light on the adverse effect of duodenal inclination on the starch digestion. As the leaning angle climbs, a growing number of starch particles are found in the proximal acid region, where enzyme activity is inhibited. The proportion of particles in the proximal region, represented by columns in Fig. 5(b), provides a quantitative evidence for this observation.

Fig. 5(c) shows the average residence time and digestion ratio of particles exiting the duodenum between 600 s and 800 s. An increase in the leaning angle negatively impacts on the digestion ratio, indicating less granular change during this period. As the leaning angle increases from 0° to 67.5°, particles pass more quickly through the duodenum because the height difference between the bottom and the outlet lowers. The combined effect of shortened residence time and a worsening digestive environment gives rise to a reduction in the digestion ratio. However, when the C-shaped tube further rotates to a lying posture (i.e., 90°), the average residence time goes up resulting from the loss of the gravitational acceleration in the proximal segment. This suggests that the primary mechanism impairing hydrolysis performance in a lying system is the inhibited enzymatic reaction, due to a higher proportion of particles distributed in the acidic environment.

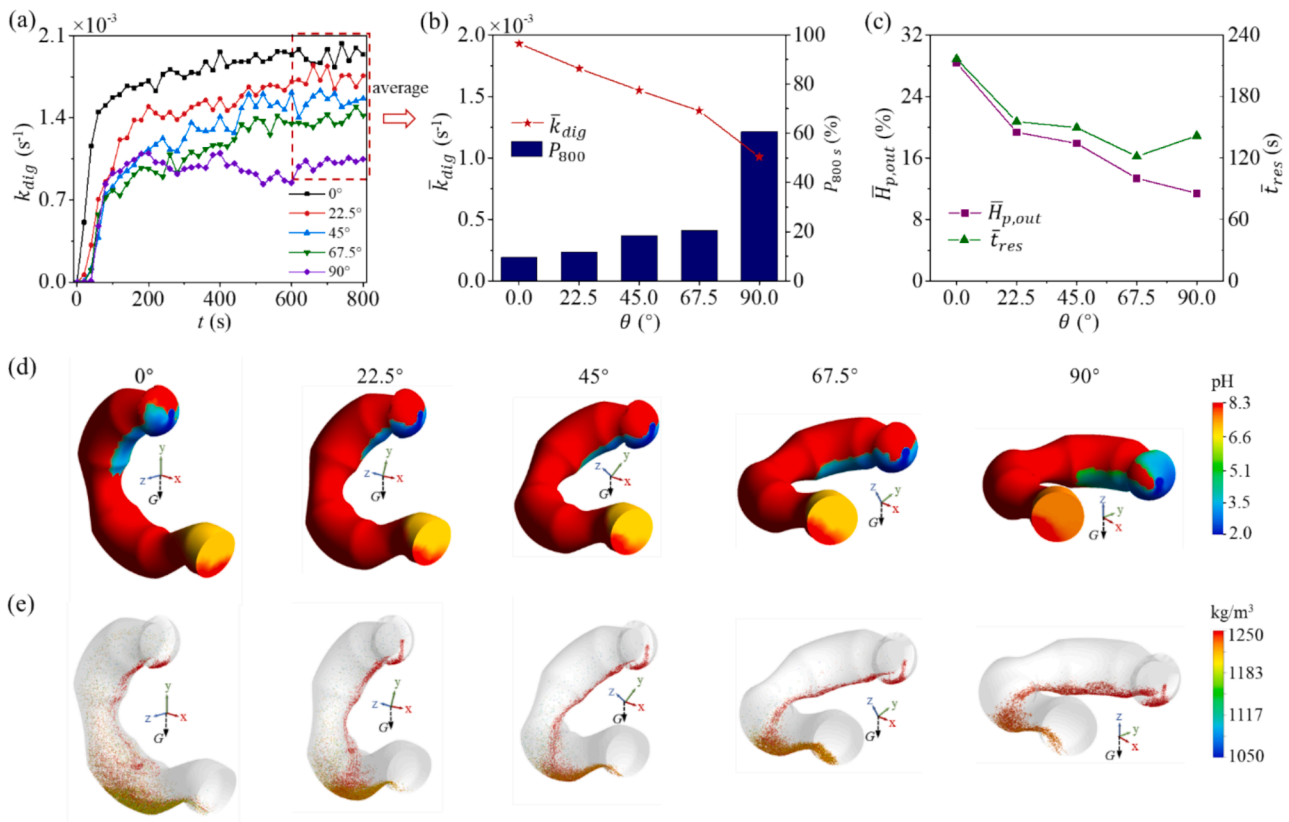


Fig. 5. Simulation results for different duodenal postures. (a) evolution of digestion rate coefficient. (b) average digestion rate coefficient from 600 s to 800 s as well as proportion of particles in the proximal region at 800 s. (c) average residence time and average digestion ratio of particles exiting the duodenum (d) pH distribution at 800 s (e) particle distribution at 800 s.

Regarding the relationship between the postprandial posture and food digestion, previous clinical studies primarily focused on the mechanisms in the stomach [44–46]. This study is the first to explore the postural effects on the digestion process in the duodenum, which is a crucial organ with multiple functions as well. The finding presents a positive impact of the standing posture on starch digestion rate in the duodenum. However, faster duodenal digestion does not necessarily lead to more digestion in the entire digestive tract. Hirota et al. [44] suggested that a postprandial supine posture, due to delayed gastric emptying, could increase the overall digestion amount of dietary carbohydrates throughout the gastrointestinal tract.

3.3. Effect of gastric acid concentration

The acidity of chyme emptied from the stomach varies with food property and meal timing [24]. Among the cases formulated in the system specifications section, the influences of gastric acidity on digestion under leaning angles of 0° (standing posture) and 90° (lying posture) were selected for detailed analysis.

The temporal evolutions and averages of the digestive rate coefficient for different inlet concentrations of hydrochloric acid are plotted in Fig. 6(a) & (b), respectively. In a standing posture ($\theta = 0^\circ$), an increase in the inlet acid concentration has a slightly negative effect on the average coefficient when the concentration is below 25 mmol/L. The corresponding pH distributions in Fig. 6(c) show that at 800 s, the acidic region gradually expands as the inlet acid concentration increases, while the bottom space of the duodenum remains alkaline. The majority of particles, which deposit at the bottom, are thus hydrolyzed by the enzyme with high activity. For the case with an inlet acid concentration of 30 mmol/L, the digestion rate coefficient in Fig. 6(a) sharply decreases at around 560 s and subsequently maintains at an extremely low

level. Consequently, Fig. 6(b) presents a notable reduction in the average value when C_{HCl}^0 rises to 30 mmol/L. This phenomenon can be understood by analyzing the temporal variation of pH distribution (see Supplementary Material, Fig. S3). The bottom region, where most starch-based particles accumulate, becomes acidic from 560 s, creating an unfavorable environment for starch digestion. By contrast, the average digestion rate coefficient in a lying posture experiences a decline at an almost steady slope. Fig. 6(c) shows that even in the 30 mmol/L case, there is still a small alkaline region at the bottom of the distal duodenum, providing a high enzyme activity region for some particles. This difference from the standing posture reflects the adverse impact of the lying posture on acid-base mixing.

Excess gastric acid is a contributor to functional dyspepsia, and patients commonly take medications, e.g., proton pump inhibitors (PPIs) and H_2 receptor blockers, to suppress or neutralize gastric acid [47]. The results presented here suggest that altering body posture may be a potential alternative to alleviate the symptom of functional dyspepsia, particularly for carbohydrate-rich meals. A lying position could help maintain a certain level of starch digestion ability in the duodenum, even with excessive inflow of gastric acid.

3.4. Biparametric orthogonal analysis

The joint effect of duodenal posture and gastric acid concentration is analyzed further according to the experimental design outlined in the system specification section. Fig. 7(a) presents the average digestion rate coefficients for all thirty cases. It is evident that, regardless of the leaning angle, the digestion rate is inhibited by an increase in gastric acidity. Regarding the impact of duodenal posture, a negative trend is observed in cases with low gastric acid concentration, i.e., $C_{HCl}^0 < 25$ mmol/L, as previously explained.

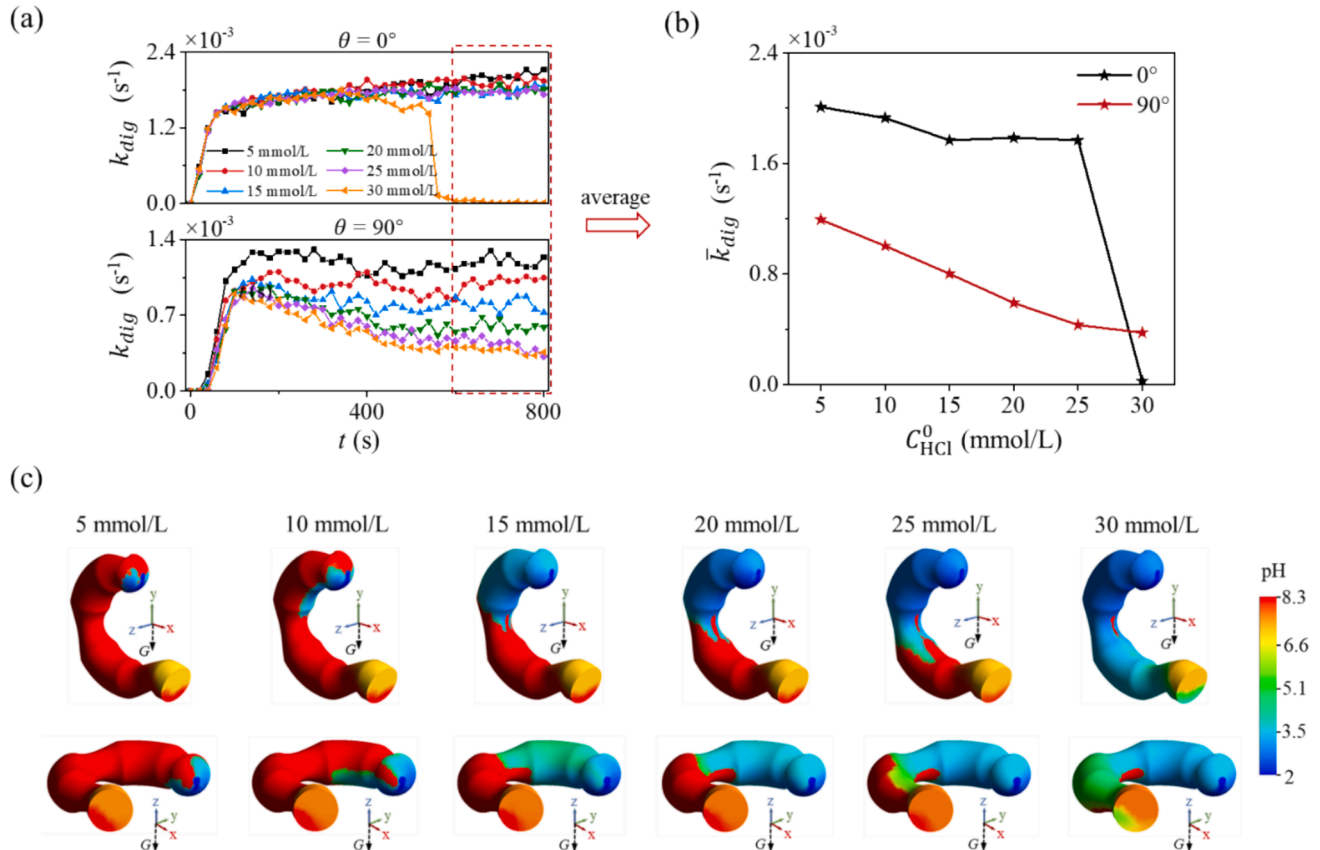


Fig. 6. Effect of gastric acid concentration in standing and lying postures on (a) digestion rate coefficient, (b) average digestion rate coefficient from 600 s to 800 s, and (c) pH distribution at 800 s.

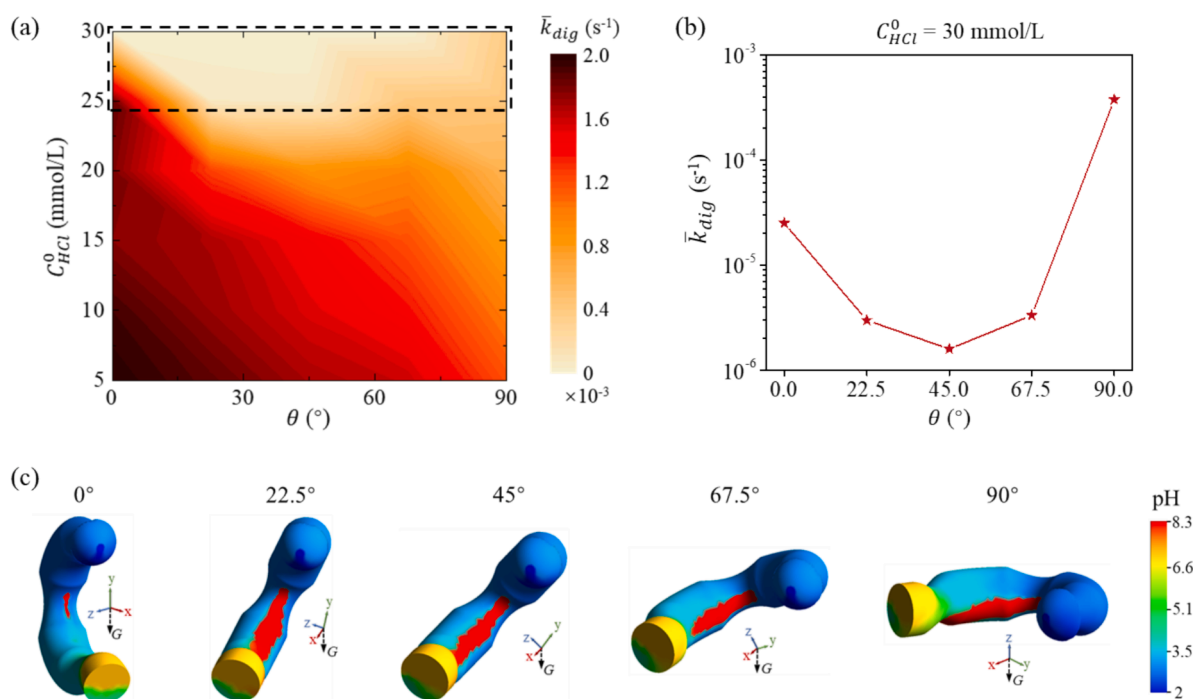


Fig. 7. (a) Effect of duodenal posture and gastric acid concentration on the average digestion rate coefficient. An example in marked region when gastric acid concentration is 30 mmol/L; (b) average digestion rate coefficient, and (c) pH distribution at 800 s.

However, both standing and lying postures (i.e., 0° and 90°) are more favorable for digestion than other postures when the acidity at the pylorus exceeds a specific threshold, as marked by a dashed box in Fig. 7 (a). Taking the case set of 30 mmol/L as an example (see Fig. 7(b)), the valley-like curve can be understood with the help of the pH distribution depicted in Fig. 7(c). As discussed in the previous section, alkaline secretion mixes more effectively with gastric acid in a standing posture, thereby creating a relatively beneficial environment for starch digestion. Meanwhile, the tilted posture leads to a banded region of unreacted alkaline fluid at the inner ring of the duodenum. In a fully lying case, some particles pass through this region, allowing them to be hydrolyzed at a higher rate.

4. Conclusion

With the objective of understanding the digestion behavior of starch-based granular food in the complex duodenal system, this study developed a 3D multi-physics model that replicated the key characteristics of the duodenum and simulated coupled fluid-particle multiphase flow along with a series of mass transfer and reaction phenomena in a near-real physiological environment. The evolutions of the digestive environment and particle properties were analyzed through in-silico experiments. The results demonstrated that the distributions of both particles and pH are crucial to the digestive efficiency of the duodenum. In a normal standing posture, most particles aggregate in the distal duodenal, where the pH level is optimal for starch digestion. As the duodenum leans, the digestion rate coefficient is restrained by up to half due to the increased proportion of particles in the proximal acid region. An increase in gastric acid concentration could effectively inhibit the digestive reaction in a lying posture. For a standing posture, a growth in the inlet acidity within a given range has little effect, but triggers a steep decline when it exceeds a threshold value.

The findings in the current work offer new insights into how human eating habits influence food digestion. The long-held belief that standing is beneficial for digestion could be supported by a new understanding. These insights will hopefully assist doctors and nutritionists in diagnosing and treating related diseases, e.g., dyspepsia. In future studies,

the effects of certain intestinal diseases, e.g., inadequate pancreatic secretion and weak wall motility, can be explored further by parametric studies. Moreover, the duodenal model developed in this study could be used to simulate the *in-vivo* delivery of drugs, particularly enteric-coated tablets, to optimize pill design and drug usage habits.

Despite reconstructing key features, this model still differs from the real duodenum in some details. For instance, microstructures on the inner wall such as folds and villi may intensify the mixing and digestive reaction in the intestine. Additionally, the presence of gas in the gut, which can influence the flow of chyme, has not been considered. Addressing these complexities will be a challenge for future research.

CRediT authorship contribution statement

Yifan Qin: Writing – original draft, Software, Methodology, Investigation, Formal analysis. **Jie Xiao:** Writing – review & editing, Supervision, Conceptualization. **Aibing Yu:** Supervision, Funding acquisition. **Xiao Dong Chen:** Writing – review & editing, Funding acquisition, Conceptualization.

Declaration of competing interest

The authors declare that they have no known competing financial interests or personal relationships that could have appeared to influence the work reported in this paper.

Acknowledgments

The authors are grateful for the financial support from the National Natural Science Foundation of China (21978184 & 22078212). Thanks also go to Particle Engineering Laboratory (China Petroleum and Chemical Industry Federation) at Soochow University. Prof. Jie Xiao acknowledges the “Jiangsu Innovation and Entrepreneurship (Shuang Chuang) Program” and the “Jiangsu Specially-Appointed Professors Program”.

Appendix A. Supplementary data

Supplementary data to this article can be found online at <https://doi.org/10.1016/j.cej.2024.156965>.

Data availability

Data will be made available on request.

References

- [1] E.N. Marieb, S. Keller, *Essentials of Human Anatomy and Physiology*, twelfth ed., San Francisco, 2018.
- [2] R. Van Buntum, M.I. Nelson, Modelling the passage of food through an animal stomach: a chemical reactor engineering approach, *Chem. Eng. J.* 166 (1) (2011) 315–323, <https://doi.org/10.1016/j.cej.2010.10.017>.
- [3] Y. Qin, X.D. Chen, A. Yu, J. Xiao, New understanding from intestinal absorption model: how physiological features influence mass transfer and absorption, *AIChE J.* 69 (8) (2023) e18099.
- [4] S. Marze, Bioavailability of nutrients and micronutrients: advances in modeling and in vitro approaches, *Annu. Rev. Food Sci. T.* 8 (2017) 35–55, <https://doi.org/10.1146/annurev-food-030216-030055>.
- [5] M.D. Sinnott, P.W. Cleary, J.W. Arkwright, P.G. Dinning, Investigating the relationships between peristaltic contraction and fluid transport in the human colon using Smoothed Particle Hydrodynamics, *Comput. Biol. Med.* 42 (4) (2012) 492–503, <https://doi.org/10.1016/j.combiomed.2012.01.002>.
- [6] N. Palmada, J.E. Cater, L.K. Cheng, V. Suresh, Experimental and computational studies of peristaltic flow in a duodenal model, *Fluids* 7 (1) (2022) 40, <https://doi.org/10.3390/fluids7010040>.
- [7] T. Zhu, A. Xia, K. Lin, Y. Huang, X. Zhu, X. Zhu, Q. Liao, Numerical investigation of bio-inspired mixing enhancement for enzymatic hydrolysis, *Chem. Eng. Sci.* 260 (2022) 117950, <https://doi.org/10.1016/j.ces.2022.117950>.
- [8] J. Zha, S. Zou, J. Hao, X. Liu, G. Delaplace, R. Jeantet, D. Dupont, P. Wu, X. Dong Chen, J. Xiao, The role of circular folds in mixing intensification in the small intestine: a numerical study, *Chem. Eng. Sci.* 229 (2021) 116079, <https://doi.org/10.1016/j.ces.2020.116079>.
- [9] Y. Wang, J.G. Brasseur, G.G. Banco, A.G. Webb, A.C. Ailiani, T. Neuberger, A multiscale lattice Boltzmann model of macro- to micro-scale transport, with applications to gut function, *Philos. T. R. Soc. A.* 368 (1921) (2010) 2863–2880, <https://doi.org/10.1098/rsta.2010.0090>.
- [10] Y. Zhang, P. Wu, R. Jeantet, D. Dupont, G. Delaplace, X.D. Chen, J. Xiao, How motility can enhance mass transfer and absorption in the duodenum: taking the structure of the villi into account, *Chem. Eng. Sci.* 213 (2020) 115406, <https://doi.org/10.1016/j.ces.2019.115406>.
- [11] N. Palmada, J.E. Cater, L.K. Cheng, V. Suresh, Modelling flow and mixing in the proximal small intestine, in: 42nd Annual International Conference of the IEEE Engineering in Medicine & Biology Society (EMBC), 2020, pp. 2496–2499.
- [12] P.V. Trusov, N.V. Zaitseva, M.R. Kamaltdinov, A Multiphase Flow in the antroduodenal portion of the gastrointestinal tract: a mathematical model, *Comput. Math. Methods Med.* 5164029 (2016), <https://doi.org/10.1155/2016/5164029>.
- [13] M. Tamura, J. Singh, L. Kaur, Y. Ogawa, Impact of structural characteristics on starch digestibility of cooked rice, *Food Chem.* 191 (2016) 91–97, <https://doi.org/10.1016/j.foodchem.2015.04.019>.
- [14] B.M.J. Martens, T. Flecher, S. de Vries, H.A. Schols, E. Bruininx, W.J.J. Gerrits, Starch digestion kinetics and mechanisms of hydrolysing enzymes in growing pigs fed processed and native cereal-based diets, *Br. J. Nutr.* 121 (10) (2019) 1124–1136, <https://doi.org/10.1017/S0007114519000503>.
- [15] D. Gidaspow, *Multiphase flow and fluidization: continuum and kinetic theory descriptions*, Academic press, 1994.
- [16] A. Guyton, J. Hall, *Textbook of medical physiology*, eleventh ed., Elsevier Inc., Philadelphia, 2006.
- [17] M. Kamaltdinov, P. Trusov, N. Zaitseva, Multi-component mixture flow in the stomach and duodenum allowing for functional disorders: results of numeric modelling for determining acidity, *Russ. J. Bio.* 21 (3) (2017) 205–223.
- [18] M.A. Van Boekel, *Kinetic modeling of reactions in foods*, CRC Press, 2008.
- [19] H.H. Sky-Peck, P. Thuvasthakul, Human pancreatic alpha-amylase. II. Effects of pH, substrate and ions on the activity of the enzyme, *Ann. Clin. Lab. Sci.* 7 (4) (1977) 310–317.
- [20] Y. Qin, J. Xiao, A. Yu, X.D. Chen, A starch digestion model considering intrinsic granular properties, *J. Food Eng.* 369 (2023) 111918, <https://doi.org/10.1016/j.jfoodeng.2023.111918>.
- [21] Y. Qin, J. Xiao, A. Yu, X. Dong Chen, Multiscale modeling of solid starch-based foods digestion in the intestinal tract for dietary property-based glycemic prediction, *Food Res. Int.* 193 (2024) 114808, <https://doi.org/10.1016/j.foodres.2024.114808>.
- [22] T.E. Moxon, O. Gouseti, S. Bakalis, In silico modelling of mass transfer & absorption in the human gut, *J. Food Eng.* 176 (2016) 110–120, <https://doi.org/10.1016/j.jfoodeng.2015.10.019>.
- [23] F. Payan, R. Haser, M. Pierrot, M. Frey, J. Astier, B. Abadie, B. Duée, G. Buisson, The three-dimensional structure of α -amylase from porcine pancreas at 5 Å resolution—the active-site location, *Acta Crystal.* 36 (2) (1980) 416–421, <https://doi.org/10.1107/S0567740880003378>.
- [24] H.P. Simonian, L. Vo, S. Doma, R.S. Fisher, H.P. Parkman, Regional postprandial differences in pH within the stomach and gastroesophageal junction, *Digest. Dis. Sci.* 50 (2005) 2276–2285, <https://doi.org/10.1007/s10620-005-3048-0>.
- [25] F.H. Martini, J.L. Nath, E.F. Bartholomew, *Fundamentals of anatomy & physiology*, Pearson Education, San Francisco, 2012.
- [26] K. Järbur, J. Dalenbäck, H. Sjövall, Quantitative assessment of motility-associated changes in gastric and duodenal luminal pH in humans, *Scand. J. Gastroenterol.* 38 (4) (2003) 392–398, <https://doi.org/10.1080/00365520310002148>.
- [27] S. Ishida, T. Miyagawa, G. O'Grady, L.K. Cheng, Y. Imai, Quantification of gastric emptying caused by impaired coordination of pyloric closure with antral contraction: a simulation study, *J. R. Society Interface* 16 (157) (2019) 20190266, <https://doi.org/10.1098/rsif.2019.0266>.
- [28] L. Ovesen, F. Bendtsen, U. Tage-Jensen, N.T. Pedersen, B.R. Gram, S.J. Rune, Intraluminal pH in the stomach, duodenum, and proximal jejunum in normal subjects and patients with exocrine pancreatic insufficiency, *Gastroenterology* 90 (4) (1986) 958–962, [https://doi.org/10.1016/0016-5085\(86\)90873-5](https://doi.org/10.1016/0016-5085(86)90873-5).
- [29] S. Standring, Gray's anatomy e-book: the anatomical basis of clinical practice, 39th ed., Spain, 2016.
- [30] J. Glaser, B. Högemann, T. Krummenerl, M. Schneider, E. Hultsch, N. Van Husen, U. Gerlach, Sonographic imaging of the pancreatic duct: new diagnostic possibilities using secretin stimulation, *Digest. Dis. Sci.* 32 (1987) 1075–1081.
- [31] P.S. Leung, *The gastrointestinal system: gastrointestinal, nutritional and hepatobiliary physiology*, Hong Kong (2014).
- [32] M. Denyer, P. Cotton, Pure pancreatic juice studies in normal subjects and patients with chronic pancreatitis, *Gut* 20 (2) (1979) 89–97, <https://doi.org/10.1136/gut.20.2.89>.
- [33] J.M. Froehlich, M.A. Patak, C. von Weymarn, C.F. Juli, C.L. Zollkofer, K.U. Wentz, Small bowel motility assessment with magnetic resonance imaging, *J. Magn. Reson. Imaging* 21 (4) (2005) 370–375, <https://doi.org/10.1002/jmri.20284>.
- [34] H. Ueda, H. Ueda, Diffusion coefficients of xylose and maltose in aqueous solution, *B. Chem. Soc. Jap.* 42 (8) (1969) 2140–2142, <https://doi.org/10.1246/bcsj.42.2140>.
- [35] O.L. Lewis, J.P. Keener, A.L. Fogelson, A physics-based model for maintenance of the pH gradient in the gastric mucus layer, *Am. J. Physiol.-Gastr.* 1. 313 (6) (2017) 599–612, <https://doi.org/10.1152/ajpgi.00221.2017>.
- [36] V. Vitagliano, P.A. Lyons, Diffusion coefficients for aqueous solutions of sodium chloride and barium chloride, *J. Am. Chem. Soc.* 78 (8) (1956) 1549–1552.
- [37] S.P. Cadogan, G.C. Maitland, J.M. Trusler, Diffusion coefficients of CO₂ and N₂ in water at temperatures between 298.15 K and 423.15 K at pressures up to 45 MPa, *J. Chem. Eng. Data* 59(2) (2014) 519–525, <https://doi.org/10.1021/je401008s>.
- [38] W. Weitschies, D. Cardini, M. Karaus, L. Trahms, W. Semmler, Magnetic marker monitoring of esophageal, gastric and duodenal transit of non-disintegrating capsules, *Pharmazie* 54 (6) (1999) 426–430.
- [39] J. Worsøe, L. Fyenne, T. Gregersen, V. Schlageter, L.A. Christensen, J.F. Dahlerup, N. J. Rijkhoff, S. Laurberg, K. Krogh, Gastric transit and small intestinal transit time and motility assessed by a magnet tracking system, *BMC Gastroenterol.* 11 (1) (2011) 1–10, <https://doi.org/10.1186/1471-230X-11-145>.
- [40] S. Nagar, R.C. Korzekwa, K. Korzekwa, Continuous intestinal absorption model based on the convection-diffusion equation, *Mol. Pharmaceutics* 14 (9) (2017) 3069–3086, <https://doi.org/10.1021/acs.molpharmaceut.7b00286>.
- [41] N.D. Wright, F. Kong, B.S. Williams, L. Fortner, A human duodenum model (HDM) to study transport and digestion of intestinal contents, *J. Food Eng.* 171 (2016) 129–136, <https://doi.org/10.1016/j.jfoodeng.2015.10.013>.
- [42] M. Tamura, O. Yumi, K. Chisato, O. Yukihiro, The importance of an oral digestion step in evaluating simulated in vitro digestibility of starch from cooked rice grain, *Food Res. Int.* 94 (2017) 6–12, <https://doi.org/10.1016/j.foodres.2017.01.019>.
- [43] C. Gonzalez, D. Gonzalez, R.N. Zuniga, H. Estay, E. Troncoso, Simulation of human small intestinal digestion of starch using an in vitro system based on a dialysis membrane process, *Foods* 9 (7) (2020) 913, <https://doi.org/10.3390/foods9070913>.
- [44] N. Hirota, Y. Sone, H. Tokura, Effect of postprandial posture on digestion and absorption of dietary carbohydrate, *J. Physiol. Anthropol. Appl. Human Sci.* 21 (1) (2002) 45–50, <https://doi.org/10.2114/jpa.21.45>.
- [45] J. Valeur, A. Berstad, T. Hausken, The effect of body position on postprandial perceptions, gastric emptying, and intragastric meal distribution: an ultrasonographic study in reclining healthy subjects, *Scand. J. Gastroenterol.* 50 (2) (2015) 170–173, <https://doi.org/10.3109/00365521.2014.990506>.
- [46] A. Steingoetter, M. Fox, R. Treier, D. Weishaupt, B. Marincek, P. Boesiger, M. Fried, W. Schwizer, Effects of posture on the physiology of gastric emptying: a magnetic resonance imaging study, *Scand. J. Gastroenterol.* 41 (10) (2006) 1155–1164, <https://doi.org/10.1080/00365520600610451>.
- [47] A.C. Ford, S. Mahadeva, M.F. Carbone, B.E. Lacy, N.J. Talley, *Functional dyspepsia*, *Lancet* 396 (10263) (2020) 1689–1702.